Nanoporous sponges as carbon-based sorbents for atmospheric water generation

*Authors: Ulrich Legrand [a], Darius Klassen [a], Sean Watson [b], Alessio Aufoujal [a], Bernard Nisol [b], Richard Boudreault [c], Kristian E. Waters [d], Jean-Luc Meunier [e], Pierre-Luc Girard-Lauriault [e], Michel R. Wertheimer [b], Jason R. Tavares [a]**

Affiliations:

[a] CREPEC, Chemical Engineering Department, Polytechnique Montreal, 2500 Chemin de Polytechnique, Montréal, QC H3T 1J4

[b] Groupe des Couches Minces, Department of Engineering Physics, Polytechnique Montreal, Box 6079, Station Centre-Ville, Montreal QC, H3C 3A7, Canada

[c] Awn Nanotech, Inc., Montreal, QC, Canada

[d] Department of Mining and Materials Engineering, McGill University, M.H. Wong Building, 3610 University, Montreal, Quebec H3A 0C5, Canada

[e] Department of Chemical Engineering, McGill University, 3610 University, Montréal, QC H3A 0C5, Canada

**corresponding author email: jason-robert.tavares@polymtl.ca*

Abstract: Water scarcity threatens more and more people in the world. Moisture adsorption from the atmosphere represents a promising avenue for providing fresh water. Nanoporous sponges ("NPS"), new carbon-based sorbents synthesized from the pyrolysis of resorcinol-formaldehyde resin, can achieve comparable performance to metal organic framework (MOF)-based systems, but at significantly lower cost. Oxygen and nitrogen functionalities can be added to the NPS surface, through oxidation or addition of phenanthroline to the initial reagent mixture, respectively. The resulting NPS sorbents have high specific surface areas of 347 to 527 $m^2 \cdot g^{-1}$ and an average capillary-condensation compatible pore size of 1.5 nm. When oxidized, the NPS can capture up to 0.28 g of water per gram of adsorbent at a relative pressure of 0.90 (0.14 $g \cdot g^{-1}$ at $P/_{Psat} = 0.40$), and maintain this adsorption capacity over multiple adsorption / desorption cycles. Scale-up synthesis of the NPS was performed and tested in an experimental water capture set-up, showing good agreement between small- and larger-scale adsorption properties. Water adsorption isotherms

fitted with the theoretical model of Do and Do demonstrate that hydroxyl functionalities are of key importance to NPS behavior.

Keywords: Water adsorption, Nanoporous sponges, Carbon-based adsorbent, Capillary condensation.

Graphical Abstract:

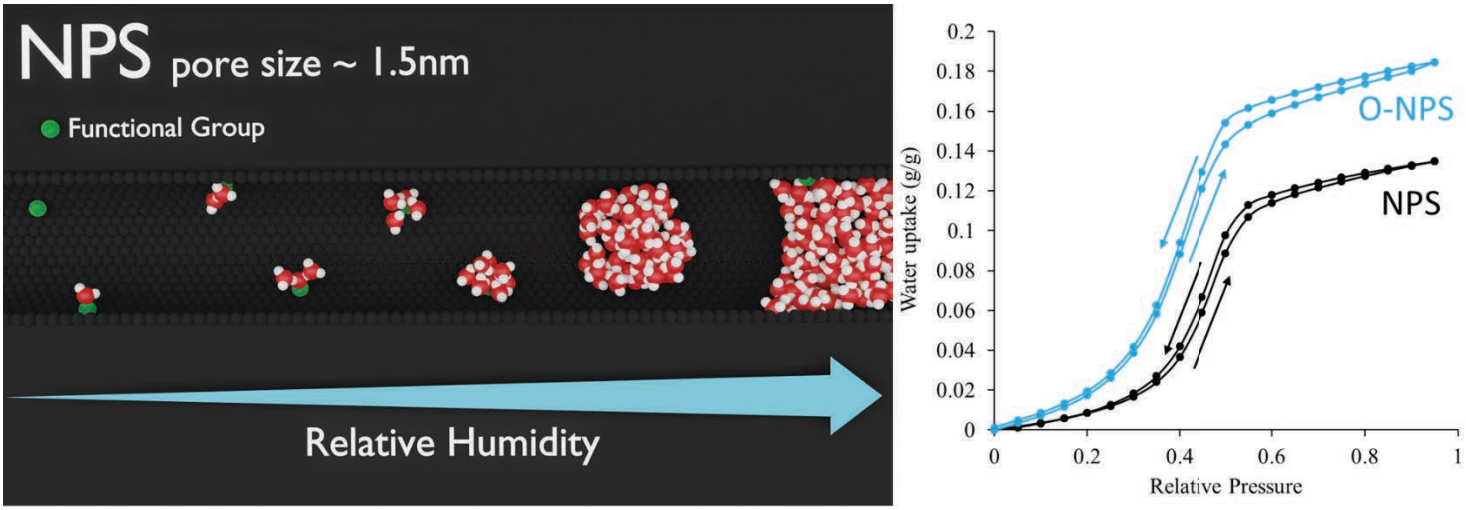

1. Introduction

Large human populations living in arid parts of the world depend either on water supplied by expensive and intermittent tankers, or groundwater, which is not always suitable for drinking. A recent UN Water Crisis Report prepared by the Food and Agriculture Organization shows that there is a growing global water crisis,[1] and that more than 2 billion people living in arid regions are already threatened by a water shortage, with an expected increasing number of people affected by the situation. Non- and semi-arid regions are also threatened. Cape Town is a striking example, with a water crisis that occurred between 2017 and 2018 due to severe droughts as well as poor governmental management and a long-term demand superior to the supply.[2] Worldwide groundwater resources are depleting at a rate that more than doubled between 1960 and 2000.[3]

Because an adequate supply of clean drinking water is a basic necessity for human survival, solutions to this growing crisis are required to avoid a catastrophic outcome. Various methods exist to generate fresh water, and most focus on using abundant seawater. Desalination removes salts and minerals from seawater to render it drinkable through thermal methods (multi flash distillation, multi effect distillation) or filtration approaches (electrodialysis, reverse osmosis).[4] Today, the leading process for intensive production of freshwater is reverse osmosis (RO),[5] which has become increasingly cost-effective over the past decade. However, RO requires the ready availability of energy (between 17 and 83 kWh per m^3),[6] together with large bodies of saline or brackish water, a distribution infrastructure and high upfront capital cost. Freshwater can be generated from humid air, but this typically requires scalable dehumidification devices in addition to high energy expenditures to cool the air below its dew point, namely between 270 and 550 kWh per m^3 of captured water.[6]

An alternative to desalination and dehumidification is water capture through adsorption. The challenge here is to generate materials on which humidity adsorption can occur without the need for cooling below ambient temperature. Adsorption and desorption on porous materials for atmospheric water harvesting above the dew point relies on the principle of capillary condensation (CC);[7] hereby, a gas-to-liquid phase transition of an adsorbate on a porous material can occur under certain conditions. CC happens at a vapor pressure lower than the saturation value (i.e. the dew point) and its efficiency is directly related to the type of adsorbate, the porous material, its average pore diameter and pore size distribution, as well as the gas temperature.[7]

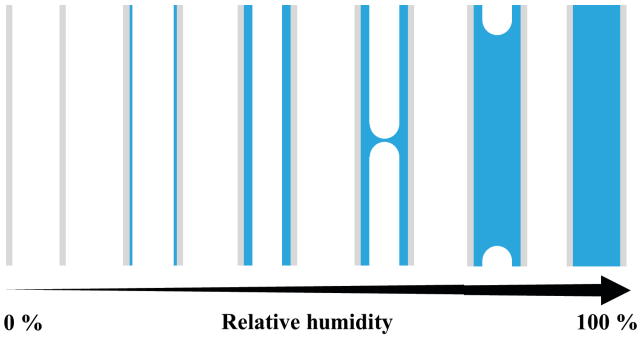

Figure 1: Capillary condensation process depending on the relative vapor pressure, inspired from Sundararajan *et al.*[8]

At low vapor pressure (i.e. low relative humidity, RH), the gas first forms a monolayer of (water) molecules adsorbed on the inner surfaces of the pores, followed by growth of a metastable multilayer (**Figure 1**). Instability of the adsorbed multilayer results from a competition between the potential energy of adsorption of the substrate with the surface energy of the film, and capillary evaporation, which occur simultaneously. At a "critical" thickness, liquid bridges can grow and form menisci, the curvature of which depend on the equilibrium vapor pressure and the surface tension of the liquid phase.[9]

An important phenomenon impacting the use of CC in water harvesting is irreversibility between the adsorption and desorption phases. This is revealed by hysteresis on the adsorption isotherms. The exact cause of hysteresis is still under debate, although several hypotheses have been evoked, such as pore blocking, cavitation, irregularities in pore shapes, inhomogeneity of surface chemistry, and mechanical deformation of pores during condensation.[10] Hysteresis is undesirable because it limits the amount of adsorbate that can be contained in the porous material, and because it leads to higher energy requirement during desorption.

Hysteresis can be prevented by aiming for pore diameters smaller than the critical one, and for an operating temperature above the critical value. These critical values are specific to the particular gas phase, namely equal to 3.0 nm for Ar at 77 K,[7] and 2.2 nm for water at 298 K.[11] The pore size distribution also influences the shape of the hysteresis, a narrow distribution being desirable to obtain smaller hysteresis.[10]

Current research on CC-based water harvesting is mostly focused on Metal Organic Frameworks (MOFs), highly porous materials based on a network of metal ions coordinated to organic ligands. Porosity is controlled via the choice of metal ions and organic ligands, as well as by the particular fabrication parameters. MOFs are synthesized through solvothermal processing, whereby crystals grow slowly from hot solutions over the course of hours to days.[12,13] While this can lead to a tightly controlled porosity, the process is difficult to scale up; ongoing research aims to accelerate crystal growth with the help of microwave irradiation or electrochemistry.[14,15] Further, as MOFs are made of coordinated ions, they can be affected by the presence of water. An important parameter to consider in regard to MOFs for water capture is their hydrolytic stability, their possible degradation in the presence of water[12] – it is not uncommon to observe a decrease in performance over multiple adsorption/desorption cycles.[16] However, optimized MOFs can display water uptakes that exceed

1 g/g at high relative pressure.[12] To a lesser extent, Covalent Organic Framework (COFs) attracted some attention in water adsorption but generally suffer from poor hydrolytic stability.[17] Some studies have tended towards carbonaceous sorbents in order to overcome the above-described stability issues and difficulty to scale up fabrication.[18] Overall, an ideal sorbent for atmospheric water capture should have high water uptake, low energy requirement, fast kinetics and stability over adsorption/desorption cycles.[19]

With those considerations in mind, a carbon-based adsorbent is discussed in the present work: nanoporous sponges (NPS) are heat-treated resorcinol-formaldehyde resins, preferably with oxygen (O) and/or nitrogen (N) functionalities added on their surface. Carbonized resorcinol formaldehyde (RF) resins have already been reported in the literature for supercapacitor and CO_2 adsorption applications.[20–22]. Pyrolyzed RF resins,[23,24] with the presence of melamine,[25,26] or urea,[27] have also been investigated as water sorbents, but mostly under the form of monoliths and for adsorption heat pump applications. We have performed physical characterization of the NPS sorbent, determined its water harvesting capabilities, and have applied a theoretical model to better grasp underlying fundamental mechanisms. NPS synthesis has also been scaled up over two orders of magnitude and resulting water harvesting properties have been validated in the laboratory.

2. Materials and methods

2.1. NPS Material synthesis

NPS is resorcinol-formaldehyde (RF) resin that has undergone high-temperature heat treatment. The resin is synthesized through wet chemistry, whereby R, F and a catalyst (sodium carbonate) are dissolved in a 1:1 mixture of water and ethanol. By heating at 80 °C over 24h, R and F polymerize to form a porous matrix, and the solvent is evaporated (**Figure 2**). It is recognized in the literature that the pore size of RF-resins depends on the R/F ratio, nature of the catalyst and

viscosity of the solution.[28] Trace amounts of catalyst are required for the resin to be cured. We chose a mass ratio of R/F/sodium carbonate of 2:3:0.01.

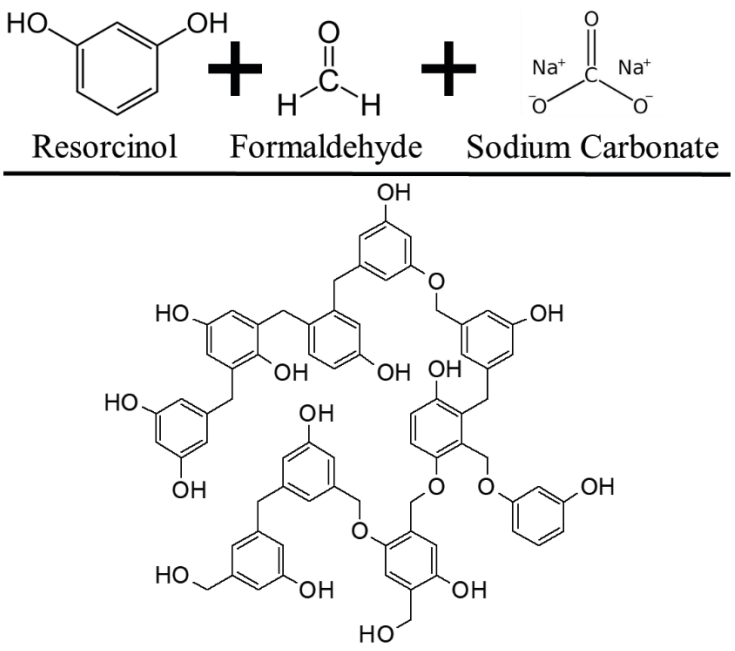

Figure 2: Reagents (top) for the synthesis of resorcinol-formaldehyde resin (bottom).

Following this, pyrolysis at 700 °C for 1h in an inert atmosphere carbonizes the resin, thereby forming a NPS sample. Pyrolysis causes pores to shrink to the required size. However, a secondary (unfavorable) effect of pyrolysis can also be observed: most of the O-based functional groups initially present in the resin are eliminated by the heat treatment, leaving a material with 95 wt% of carbon. Functional groups are beneficial to promote water nucleation on the accessible surface.[18] In order to improve the concentration of functional groups in NPS in the form of N- and O-moieties, we have included the following suitable variations in the synthesis protocol:

A first approach consisted of including an additional molecule containing N-functional groups, phenanthroline, into the original reagent mixture before curing and pyrolyzing the resin. This compound was chosen for its molecular structure, ability to incorporate into the carbon matrix,[29]

and its mass concentration was selected at 40 wt% relative to the RF-resin. Following this technique, N-functionalized NPS (N-NPS) samples were produced. A second approach was to add O-functionalities whereby the material was heated at 700 °C for 1h in the presence of air, leading to O-NPS. Finally, we combined the two approaches to obtain N/O-functionalized NPS (NO-NPS).

2.2. Physical characterization

NPS samples were characterized by their pore size, pore volume and specific surface area using the Brunauer-Emmett-Teller (BET) technique. A *Quantachrome Autosorb-1* gas sorption analyzer measured the evolution of mass uptake as a function of relative pressure of N_2 (the adsorbate gas), at constant T = 77K, after degassing overnight at 200 °C under vacuum. Elemental compositions of the NPS surfaces and bulk were determined using X-Ray Photoelectron Spectroscopy (XPS) and elemental analyses. XPS was performed on a *Scientific K-Alpha* XPS system from Thermo Scientific. Monochromated Al Kα X-rays, producing photons of 1486 eV acquired at normal angles to the surface were used on 400 μm diameter spots. Wide scans with step size 1 eV, pass energy 160 eV, dwell time 200 ms and in the range 1350 to 0 eV were acquired for each sample. The binding energy scale was calibrated with respect to the carbon (C 1s) peak at binding energy, BE = 284.6 eV. C1s high-resolution (HR) core-level spectra were also acquired. Atomic concentrations were calculated using the CasaXPS software (Version 2.3.23). The elemental analyses were performed on a *Truspec* Micro analyser from LECO, to determine the relative concentrations of C, H, and N, based on infrared sensors (to detect gaseous CO_2 and H_2O), and a thermal conductivity sensor for N_2. The complementary module *Micro O* from LECO detected CO_2 with an infrared sensor, to determine O concentrations. The NPS samples were analyzed by scanning electron microscopy (SEM) using a JEOL 7600TFE instrument, operated at 10 kV, as well as a Hitachi S-4700 instrument at 3 kV.

2.3. Water adsorption

The NPS samples were tested in a custom-made environmental chamber with controlled RH and temperature, performed at P/P_{sat} = 0.90 and T = 25 °C. NPS masses of 10 to 100 mg were initially dried in an oven at 150 °C before being placed in a petri dish into the environmental chamber. Samples were weighed prior to the test and every 10 min thereafter to determine the mass evolution over time. Adsorption isotherms were obtained on a dynamic vapor sorption (DVS) *Intrinsic* instrument from Surface Measurement Systems Ltd., UK. Samples were equilibrated at P/P_{sat} = 0.00 to determine dry mass, followed by increments of 0.05 to 0.95, and then brought back down to 0.00 for desorption measurements. The mass change was recorded at each increment once equilibrium was reached, overall error being ±0.1 µg. Due to insufficient availability of DVS equipment and of scalability tests, the environmental chamber was combined with a fully automated gravimetric equipment (**Figure S1**). The resulting automated environmental chamber was subsequently used to measure all isotherms of scaled-up samples and all adsorption/desorption cycles.

2.4. Fitting of the adsorption isotherms

The experimentally-determined adsorption isotherms have been fitted to the theoretical equation of Do and Do, modified by Neitsch et al. (DDN).[30–33] This equation describes the adsorption process of H_2O on C as a two-step mechanism, where the first step corresponds to adsorption of water molecules on primary sites (functional groups) on the surface (**Figure 3**). Water clusters then grow around these primary sites via hydrogen bonds. The second step occurs when clusters reach a threshold size of 6 molecules and break down into water pentamers that fill the micropores. It has been shown by Neitsch et al. that pentamers can be generalized into m-mers ($m \geq 5$) for higher accuracy.[31]

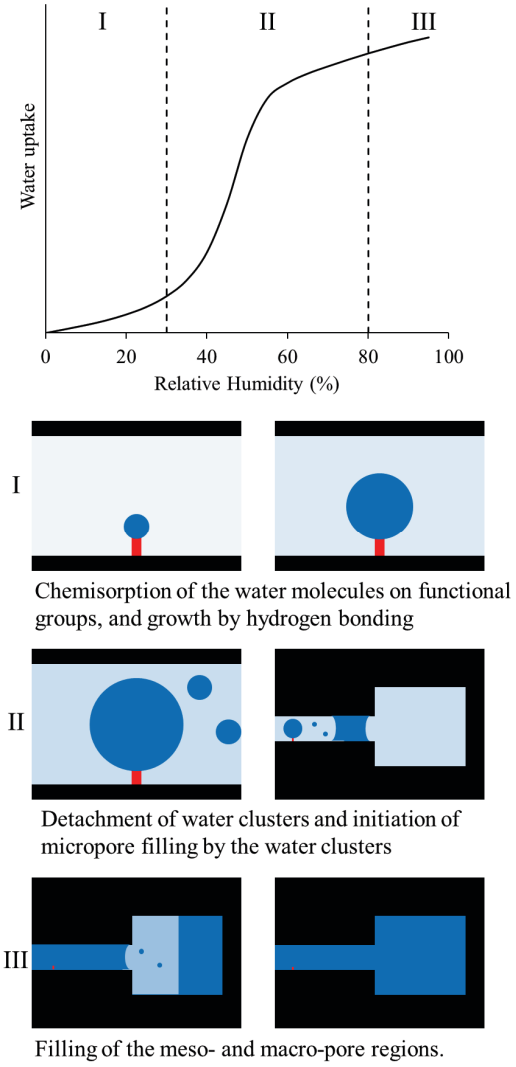

Figure 3: Schematic representation of three regions that characterize water adsorption on microporous carbon-based material such as the NPS.

The equation describing water adsorption is:

$$a = a_0 \frac{K_f \sum_{n=1}^{N} n h^n}{1 + K_f \sum_{n=1}^{N} h^n} + a_{\mu s} \frac{K_\mu h^m}{1 + K_\mu h^m} \qquad \text{(Equation 1)}$$

where a is water uptake, a_0 is the concentration of surface active sites, $a_{\mu s}$ is the saturation concentration in the micropores (all three in units of mol·g^{-1}); K_f is the chemisorption equilibrium constant, K_μ is the micropore equilibrium constant; N is the maximum number of water molecules adsorbed per surface site; m is the size of the water m-mers that desorb from clusters and fill the micropores; and h is the relative pressure. To fit experimental data with the theoretical equation, we used the least-square method with the determination coefficient R^2, as follows:

$$R^2 = 1 - \frac{\sum(a_{exp} - a_{th})^2}{\sum(a_{exp} - \overline{a_{exp}})^2} \qquad \text{(Equation 2)}$$

where a_{exp} represents experimental data, a_{th} the corresponding theoretical data, and $\overline{a_{exp}}$ the average of experimental data over the relative pressure range.

2.5. Water capture device

The water adsorption properties of non-functionalized NPS measured with small scale (< 100 mg) samples were validated on a larger scale with a custom-made water capture set-up (**Figure S2**): Moist air is generated with air bubbling through water whose temperature is controlled using a boiler and passed through the porous material at a controlled flow rate, until saturation occurs. The NPS is contained in a column insulated with glass wool. Water desorption is accomplished through mild heating with a heating tape coiled around the column, the desorbed molecules then being condensed with a water-cooled condenser.

The laboratory-scale water capture set-up was first validated with a well-known desiccant (silica gel) used as a control adsorbent. This device can accommodate up to 50 g of NPS, and can accurately measure the amount of water collected per adsorption / desorption cycle (± 0.01 g).

3. Results and discussion

3.1. Porosity and structure

Minimal hysteresis is observed between the adsorption and desorption isotherms when using N_2 (shown in **Figure S3**).

Table 1: Summary of surface area, pore size and pore volume for the various NPS samples with N_2 gas adsorbent.

Sample	NPS	N-NPS	O-NPS	NO-NPS
Surface area ($m^2 \cdot g^{-1}$)	487	347	484	527
Average pore size (nm)	1.5 ± 0.2	1.5 ± 0.2	1.7 ± 0.2	1.7 ± 0.2
Pore volume ($cm^3 \cdot g^{-1}$)	0.276	0.231	0.286	0.321

The NPS samples exhibit high available surface areas and an average pore size of less than 2 nm (**Table 1**), below the critical value of 2.2 nm for water adsorption at 298 K.[11] A key aspect for reversibility between the adsorption and desorption curves is the pore size distribution. The NPS samples exhibit a very narrow pore size distribution (**Figure S4**), favouring reversibility.

The treatments leading to NPS samples with N and O-functional group additions initially appear to have little effect on porosity. However, Figure S4 shows a larger proportion of pore sizes greater than 2.2 nm in the case of N-NPS samples.

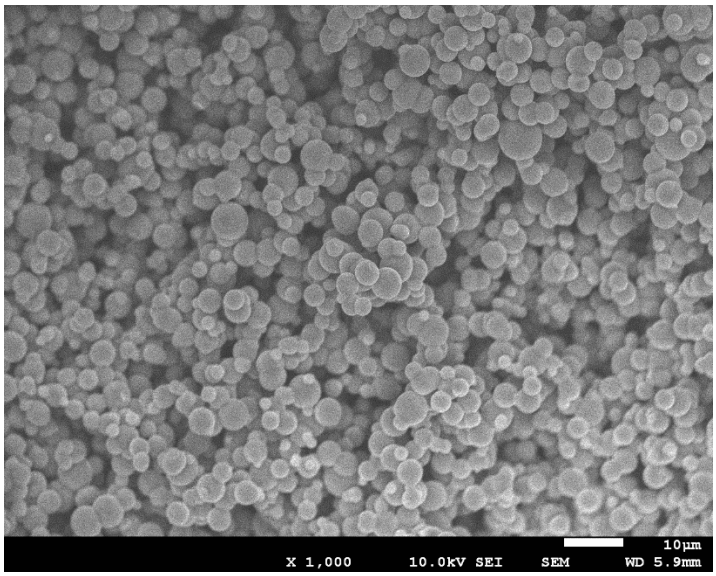

Figure 4: SEM micrograph of a non-functionalized NPS sample (scale bar is 10 µm), synthesised in diluted conditions.

The micrometric structure of non-functionalized NPS, shown in **Figure 4**, reveals spherical-shaped particles with a mean diameter of 3.7 ± 1.1 µm. These micro-particles are thought to have this specific shape on account of the synthesis process, whereby resorcinol and formaldehyde are polymerized in dilute solutions.[34] The micro-particles agglomerate through complete evaporation of the solvent, and they maintain their shape in the course of heat treatments. These particular micro-spheres are observed when the precursors are diluted in the water/ethanol solvents (concentrations lower than 0.1 $mol \cdot L^{-1}$). When synthesizing larger batches of NPS samples, the precursors have been more concentrated in order to decrease the solvent volume needing to be evaporated, with precursor concentrations around 1 $mol \cdot L^{-1}$. Then, the spherical microstructure was not observed anymore (**Figure S5**). The synthesis under concentrated conditions leads to larger macro-metric blocks that were then crushed into a finer powder. It should, however, be noted that these samples with larger structure exhibited similar porosity compared to their micro-spherical counterparts.

3.2. Chemical composition

Typical XPS surveys spectrum are shown on **Figure S6**, corresponding to peaks of carbon C 1s, nitrogen N 1s and oxygen O 1s. The elemental concentrations of the four types of NPS samples are summarized in **Table 2**.

Table 2: Summary of carbon, oxygen and nitrogen surface concentrations of the four different NPS sample types.

	C1s (at%)	O1s (at%)	N1s (at%)
NPS	93.8 ± 0.3	6.2 ± 0.3	-
N-NPS	92.0 ± 2.1	5.1 ± 1.7	2.9 ± 0.4
O-NPS	93.0 ± 0.1	7.0 ± 0.1	-
NO-NPS	88.5 ± 0.4	7.1 ± 0.5	4.4 ± 0.1

XPS results show that N is indeed added to the material's structure and remains present even after pyrolysis. O concentration [O] is slightly increased after the oxidation step. An increase in N concentration [N] for NO-NPS, is most likely explained by mass loss during heat treatments. Indeed, an 80% mass loss is observed after pyrolysis, while an additional 60% loss from the remaining material is observed after the oxidation step. Since phenanthroline can incorporate into a carbon matrix during pyrolysis,[35] one can expect [N] to increase after the oxidation step. Peak-fitting of the high-resolution C1s peak (**Figure S7**) shows that the majority of C is graphitized through pyrolysis, with more than 80% of C in the sp^2 hybridized form.

The elemental compositions of bulk NPS were obtained with a CHN analyzer. The resulting weight concentrations were converted into atomic concentrations to allow comparison with the corresponding surface compositions (**Table 3**), once the hydrogen concentration was excluded. Overall, [O] is seen to be more abundant on the surface than in the bulk, because oxidation

proceeds mainly on the former. The [N] is similar in the bulk and surface cases, as expected from the addition via phenanthroline, because after initial mixing with the other reagents, it became fully incorporated into the solid. One can note that nitrogen and oxygen can also be incorporated through the initial addition of melamine or urea to the RF resin, the carbon activation with CO_2 or its impregnation with KOH.[25-27]

Table 3: Bulk elemental compositions of the four different NPS sample types. The error on the values is lower than 0.1 at%.

	Carbon (at%)	Oxygen (at%)	Nitrogen (at%)
NPS	99.2	0.8	-
N-NPS	96.6	1.1	2.3
O-NPS	97.7	2.3	-
NO-NPS	86.0	9.7	4.3

3.3. NPS water uptake measurements in the environmental chamber

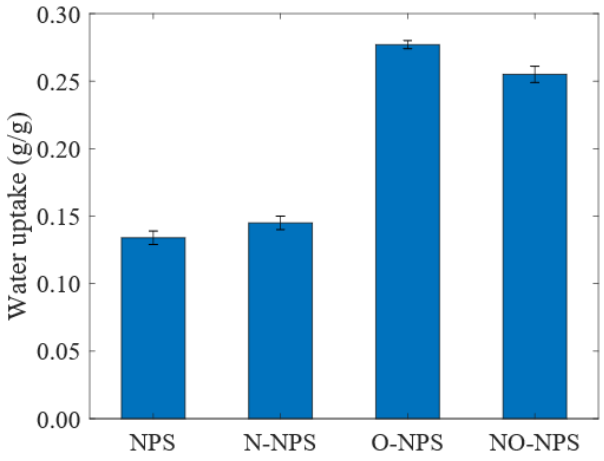

Figure 5: Preliminary water uptake measurements for the four NPS sample types at P/P_{sat} = 0.90 / 25 °C. Error bars correspond to the average of 3 measurements.

The oxidation step appears to play a key role in increasing water uptake among the different sample types (**Figure 5**); the water uptake is seen to have almost doubled after oxidation, and almost reached the full water uptake capacity measured by BET analysis that is equal to 0.286 $cm^3 \cdot g^{-1}$ for O-NPS (see Table 1). Conversely, at $P/P_{sat} = 0.90$, N addition did not appear to have a significant effect on water uptake. Because water harvesting sorbents are particularly relevant at low relative pressure, the two best-performing samples were also tested at $P/P_{sat} = 0.40$, where O-NPS and NO-NPS showed respective water uptake values of 0.14 and 0.21 $g \cdot g^{-1}$. At this lower relative pressure, N functionalities seemed to improve the performance. However, the adsorption kinetics at $P/P_{sat} = 0.40$ were slower and it took almost 40 min to reach a plateau, compared with 10 min at $P/P_{sat} = 0.90$ (**Figure 6** and **Figure S8** for O-NPS).

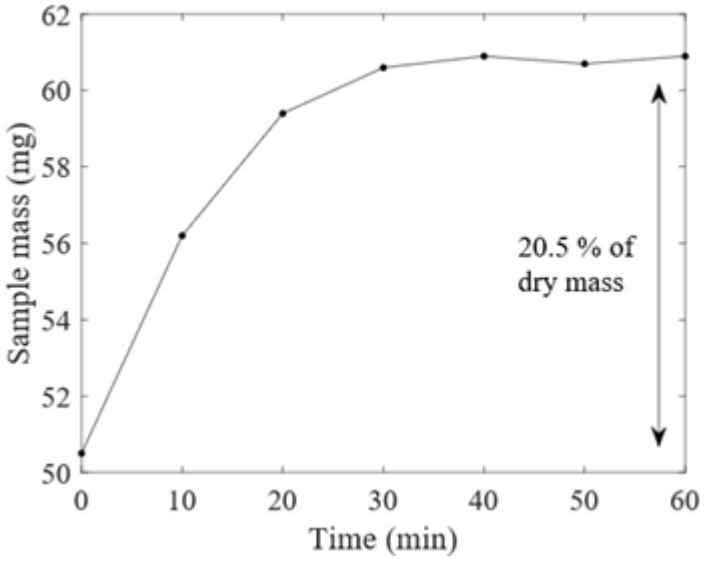

Figure 6: Water adsorption versus time for an NO-NPS sample at P/Psat = 0.40 / 25 °C.

3.4. Adsorption isotherms and theoretical aspects

Isotherms of the four sample types were obtained using the DVS Intrinsic (**Figure 7**), so as to characterize water uptake from P/Psat = 0.00 to 0.95, along with hysteresis between the adsorption

and desorption portions. NPS and O-NPS are seen to display a type V isotherm (IUPAC classification) with little to no hysteresis, while N-NPS and NO-NPS have type VI isotherms with a H3 hysteresis loop. This type of loop is generally associated with non-rigid aggregates of plate (oblate spheroid)-like particles.[36,37] From these isotherms, it appears that O in the material increases overall water uptake, a result already observed with the environmental chamber and resulting from affinity between water molecules and highly polar O functionalities (attractive dipole-dipole interactions, hydrogen bonding). In contrast, N seems to have a more complex role since water adsorption occurs at higher relative pressure and the isotherm presents stronger hysteresis. One can also note that samples had higher water uptake values when measured in the environmental chamber, except for the case of non-functionalized NPS. Reasons for this difference may include RH error in the environmental chamber (± 2%) that would particularly affect samples containing N. Indeed, at P/Psat = 0.90, a small variation will lead to a greater variation of water uptake for the N-functionalized NPS compared to the others. Other causes for this difference include potential over-estimation of water uptake in the environmental chamber, and inhomogeneity of the functionalized materials, considering that sample masses of less than 25 mg were analyzed with the DVS.

Kinetics were also extracted for NPS and O-NPS from the raw data of the DVS (Figure S9) in the P/P_{sat} range from 0.35 to 0.60. This corresponds to the range where the highest water uptakes are observed. Kinetics were assessed for each increment of $P/P_{sat} = 0.05$ based on two parameters: the necessary time to reach 90% of the maximum water uptake at each step, as well as the initial adsorption rate. From **Table 4**, O-NPS exhibits faster kinetics to adsorb and desorb water compared to NPS, on top of having a higher maximum water uptake.

Table 4: Kinetics data in the P/P_{sat} range of 0.35-0.60 for NPS and O-NPS adsorption and desorption.

Step	**P/P_{sat}**	**Time to reach 90% of max. uptake [min]**		**Initial slope [$g_{H2O} \cdot kg_{sorbent}^{-1} \cdot min^{-1}$]**	
		NPS	**O-NPS**	**NPS**	**O-NPS**
Adsorption	0.35	24.5	43.0	0.59	0.91
	0.40	41.5	63.1	0.67	0.96
	0.45	69.2	63.1	0.76	0.95
	0.50	75.9	41.9	0.83	0.92
	0.55	43.2	20.8	0.78	0.82
	0.60	21.0	15.0	0.60	0.67
Desorption	0.60	11.7	8.8	-0.47	-0.57
	0.55	17.3	10.8	-0.53	-0.58
	0.50	74.7	27.2	-0.63	-0.68
	0.45	92.6	79.4	-0.77	-0.85
	0.40	61.2	75.1	-0.82	-1.00
	0.35	38.9	57.2	-0.74	-1.01

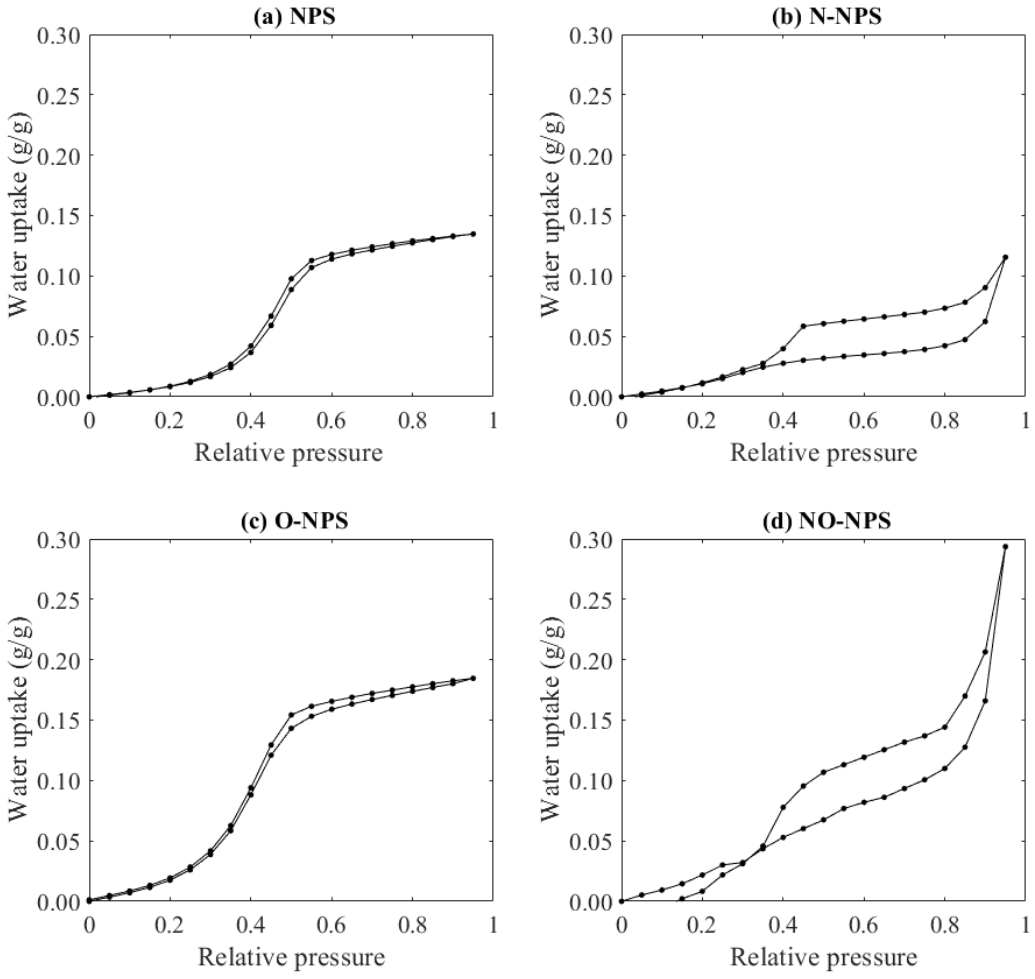

Figure 7: Adsorption and desorption isotherms for (a) NPS, (b) N-NPS, (c) O-NPS, (d) NO-NPS measured at 30°C.

Fitting the experimental data with the DDN model resulted in a strongly statistically valid fit, namely $R^2 > 0.99$, as seen in **Figure S10**. The error on the different parameters was determined from several combinations of fitting parameters, leading to the mentioned R^2 values higher than 0.99 (**Table 5**).

Table 5: Fitting parameters of the DDN model (**Equation 1**) to the water adsorption isotherms.

	Surface active site concentration a_0 (mmol·g^{-1})	Micropore saturation concentration $a_{\mu s}$ (mmol·g^{-1})	Maximum water molecules per surface site N	Water cluster size m (molecule number)	Chemisorption equilibrium constant K_f	Micropore equilibrium constant K_μ	R^2
NPS	0.42 ± 0.03	5.43 ± 0.19	11 ± 1	9 ± 0	15 ± 1	1072 ± 64	0.992 ± 0.002
N-NPS	0.25 ± 0.01	1.26 ± 0.05	172 ± 1	5 ± 0	15 ± 1	687 ± 8	0.992 ± 0.001
O-NPS	0.65 ± 0.03	7.77 ± 0.30	8 ± 0	7 ± 0	16 ± 3	570 ± 42	0.993 ± 0.002
NO-NPS	0.65 ± 0.03	3.02 ± 0.24	155 ± 3	6 ± 1	16 ± 2	703 ± 33	0.993 ± 0.002

The presence of bonded O in a sample is seen to increase the values of parameters a_0 and a_μ, while that of N in the NPS drastically changes the N parameter's value. All of these parameters are in ranges that possess plausible physical meanings,[38] and this fact can help resolve observed fundamental differences between the various structures. Table S1 summarizes the absolute concentrations of diverse functional groups, obtained by deconvoluting high-resolution XPS peaks of O 1s and N 1s. It shows a close correlation between the concentration of hydroxyl (OH) groups and the parameter a_0 that corresponds to the primary adsorption sites. This strongly suggests that OH groups are responsible as adsorption sites for the first water molecules, via hydrogen bonding; in contrast, the presence of N is seen to actually decrease the concentration of OH. The parameter $a_{\mu s}$ corresponds to the micropore filling concentration; micropores typically have sizes below 2 nm. NPS and O-NPS have 75-80% of their pores in this size range, while it is only 55% for N-NPS and NO-NPS. Micropore saturation concentration $a_{\mu s}$ is lower than expected for N-NPS, O-NPS and NO-NPS, when compared to the values obtained in the environmental chamber (Figure 5). This observation fits with the abovementioned discrepancy between the DVS and environmental chamber measurements.

The water cluster size *m* that can fill the micropores differs little between the samples, contrary to *N*, the maximum number of water molecules that can attach to a primary adsorption site through hydrogen bonds. The presence of N increases this parameter value from $N \sim 10$ molecules to more than 150. At low relative pressure, the initial adsorption steps can be described as follows: (i) a first water molecule attaches to the primary adsorption site through hydrogen bonding; (ii) subsequent water molecules become secondary adsorption sites; (iii) additional water molecules adsorb onto the secondary adsorption sites until reaching the maximum value *N*.[32] In Table S1, it can be observed that the N-containing samples have lower OH concentration. A lower concentration of hydroxyls, thus a reduced number of primary adsorption sites, allows for more physical space around each site enabling a larger number of water molecules to be attached. This is also reflected in the observation of larger pores for N-containing samples. One can suppose that the maximum *N* value results from physical blockage, governed by pore size as well as interaction with other water clusters. Indeed, large water clusters with sizes up to 280 molecules have been reported by Ludwig et al.[39] No clear tendencies can be drawn from the equilibrium constants K_f and K_μ, respectively correlated to chemisorption and micropore filling.

3.5. Scalability of NPS production

A larger batch of non-functionalized NPS was synthesized (**Figure S11**) in order to verify whether the NPS synthesis process could be readily scaled up, without a decrease in performance. While smaller samples of RF resin were easily turned into powder before pyrolysis, larger batches formed a compact, glassy material that had to be crushed into powder before heat treatment. Pyrolysis of the latter led to smaller mass loss, going from 80% to 50%, probably due to the larger particle size since the composition remained identical.

The resulting scaled-up batch of non-functionalized NPS weighed 30 g, compared with 30 to 200 mg batches tested in the environmental chamber, and less than 25 mg in the DVS. Comparison of the isotherms for small and larger batches of NPS is shown in **Figure S12**. One can note minor differences in the maximum water uptake and hysteresis that can be attributed both to experimental error and to intrinsic differences between the small and larger batch of NPS.

The larger batch was tested in the water capture set-up (Figure S2) and desorbed water collected from the condenser was weighed as a function of time, depending on the desorption temperature (**Figure 8**). Some water remained adhering to the walls of the water-cooled condenser. The weight of collected water was corrected to take this into account, by assuming a constant mass, 1.5 ± 0.1 g, of irretrievable water on the condenser walls (see further details in Supplementary Information). Water uptakes were found to be between 0.14 and 0.16 $g \cdot g^{-1}$, very close to those observed at the smaller scale.

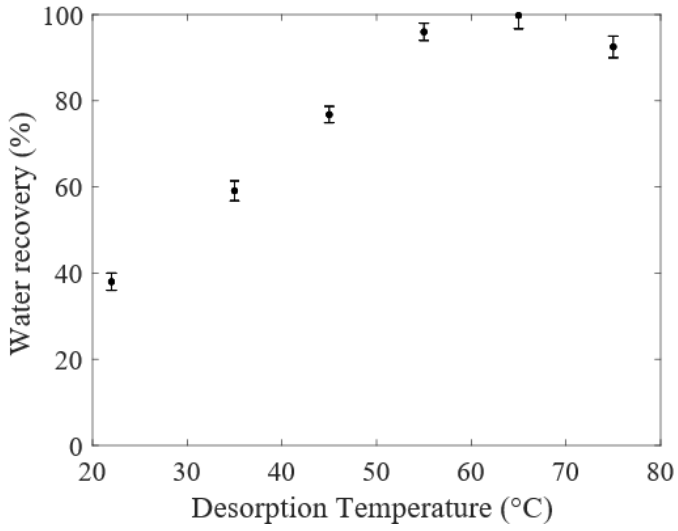

Figure 8: Desorption and recovery of water (in %) from non-functionalized NPS, presented as a function of the desorption temperature. Error bars correspond to the incertitude on the irretrievable water.

Based on these tests, the optimum desorption temperature was found to range between 55 °C and 75 °C. The water recovery values must be taken with caution due to the residual water left on the condenser walls. Mass measurements before and after desorption showed no residual water in the NPS material, even at room temperature, in agreement with the observed non-hysteretic adsorption isotherms. We believe that the observed lower % of water recovery at reduced temperature in Figure 8 is attributable to the experimental set-up rather than the material. Lower temperatures lead to less supersaturated vapor from the NPS, thus to smaller condensation.

3.6. NPS cyclability

An important practical aspect of using NPS to capture atmospheric moisture is cyclability, namely the ability to maintain constant performance over multiple adsorption / desorption cycles. We therefore tested successive cycles of adsorption in the environmental chamber and desorption in an oven, while recording water uptake for each cycle, as shown in **Figure 9a** for NPS (**Figure S13** shows O-NPS cyclability on small scale samples). The relative humidity was varied between 5 and 95 %, with the total duration being 6 h per cycle. Even after more than 60 cycles, no significant performance loss could be observed, similar to reports for several MOF sorbents.[12]

From a single adsorption/desorption cycle (Figure 9b), kinetics can be deduced. It takes respectively 62 and 72 min to reach 90% of the maximum adsorption and desorption values for a bed height of 1 mm of NPS particles. Initial rates of adsorption and desorption are similar, and respectively equal to 3.5 and -3.3 $g_{H2O} \cdot kg_{NPS}^{-1} \cdot min^{-1}$. These values are higher than those reported in Table 4, as a relative pressure increase from 0.05 to 0.95 is applied here, rather than the 0.05 to 0.95 increments in the table.

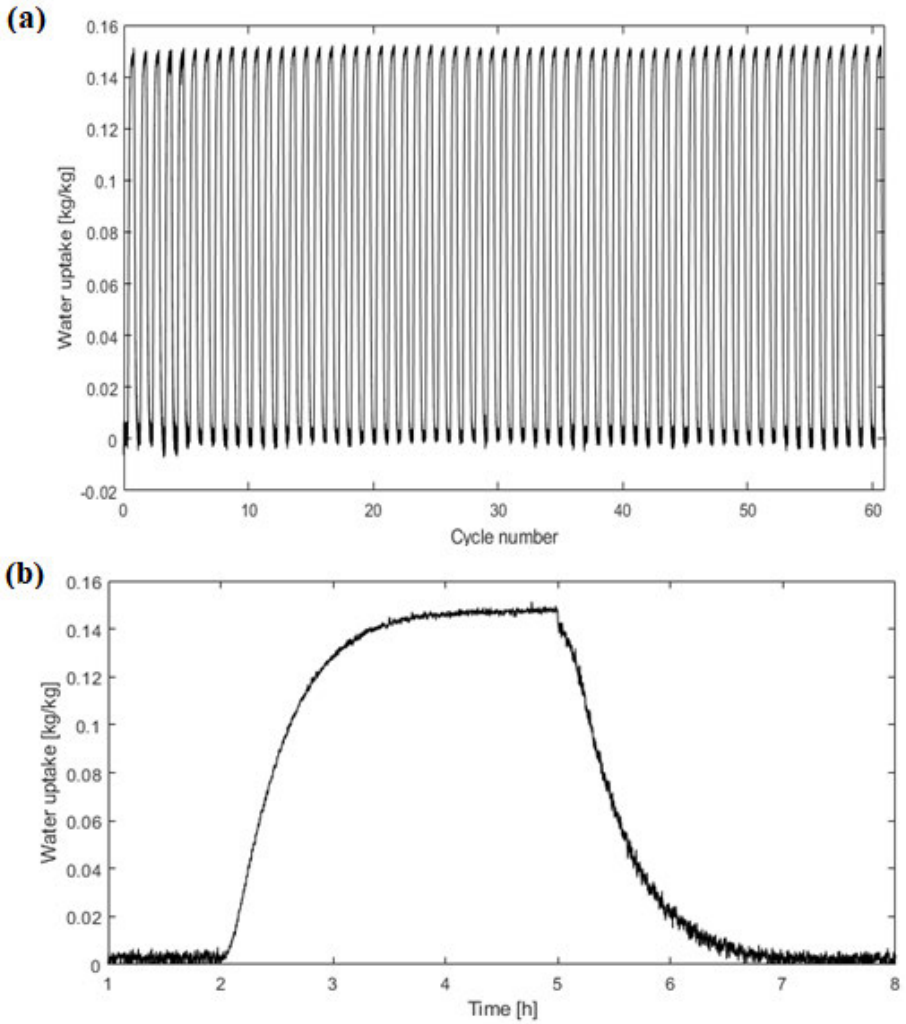

Figure 9: (a) Cycles of adsorption and desorption for the non-functionalized NPS, recorded between P/Psat = 0.05 and 0.95. (b) Enhanced view of 1 cycle.

3.7. Discussion

The water adsorption performance of the present NPS material were compared with that of other sorbents (**Table 6**), including MOFs, zeolites, mesoporous silica, and other carbon-based sorbents. This comparison focuses mainly on parameters that are relevant for large-scale implementation. The water uptake evolution over 5 cycles provides insight regarding stability over multiple adsorption / desorption cycles and is most generally reported in literature. Practical application

requires thousands of cycles and thus requires minimal performance loss from one cycle to another, a characteristic that has clearly been demonstrated for NPS (Figure 9a). The desorption temperature is the temperature required to completely regenerate the material before beginning a new adsorption cycle, and it serves as a metric to determine the amount of energy required to extract water from the sorbent. Better metrics to compare the energy consumption of sorbents are the enthalpy of adsorption and desorption. These can be obtained from thermodynamic model on isotherms at different temperatures.[40] Some recent studies consider solar energy input during diurnal cycles:[41] Cold, humid nights facilitate efficient water adsorption, while solar warmth during the day enables desorption. However, this is clearly limited to a single adsorption / desorption cycle per 24 h period. Multiple cycles per day obviously require much larger energy input for desorption, and this calls for the lowest possible regeneration temperature. One might also note that partial vacuum has occasionally been applied in previous literature, to further assist water desorption. Much to their advantage, the present NPS samples enable complete desorption at ambient pressure, 100 kPa.

Table 6: Comparison of water uptake at low and high relative pressures (P/P_{sat}), cyclability and desorption temperature of common sorbents from literature data.

Type of sorbent	Name of sorbent	Water uptake (g/g) at $P/P_{sat} = 0.3$	Water uptake (g/g) at $P/P_{sat} = 0.9$	Desorption temperature (°C)	Water uptake loss after 5 cycles (%)	Reference
Carbon-based	CMK-1	0.01	0.95	No avalaible data	No avalaible data	[42]
Al-based MOF	Basolite A100	0.06	0.25	96	36	[16,43]
Mesoporous Silica	MCM-41	0.06	0.96	225	4.2	[16,44]
Carbon-based	**Nanoporous sponges (NPS)**	**0.14 [$P/P_{sat} = 0.4$]**	**0.28**	**55**	**0**	**Reported here**
Cr-based MOF	(Cr)MIL-101	0.15	1.35	140	0	[12]
Al-based MOF	Basolite A520	0.22	0.35	70	0	[45]

Si-aluminophosphate	SAPO-34	0.22	0.24 [P/P_{sat} = 0.75]	140	0	[46]
Al-based MOF	Basolite A300	0.26	0.82	No available data	65.6	[16]
Carbon-based	PCC-1	0.26	0.33	100	0	[18]
Zr-based MOF	MOF-801	0.27	0.35	80-85	5.5	[16,47]
Al-based MOF	CAU-10	0.28	0.37	75	0.8	[16,48]
Aluminophosphate	$AlPO_4$	0.29	0.33	75	0	[49]
Al-based MOF	CAU-6	0.34	0.38	150	40.8	[16,50]
Alumina/Silica zeolite	Zeolite 13X	0.39	0.42	150	63.9	[16,51]
Cu-based MOF	Basolite C300	0.52	0.69	102	68.1	[16,43]
Ni-based MOF	Ni-MOF-74	0.55	0.62	No available data	52.0	[16]
Zr-based MOF	MOF-841	0.55	0.63	No available data	5.0	[16]
Co-based MOF	Co-MOF-74	0.57	0.63	No available data	37.6	[16]
Mg-based MOF	Mg-MOF-74	0.61	0.75	75	57.3	[16,52]

From Table 6, NPS water uptake at low and high relative pressure is seen to be lower than corresponding values reported for several other sorbents in the literature. However, most other sorbents display low stability over five adsorption / desorption cycles, as well as high desorption temperature values. This can be explained by hydrolytic instability, the adsorbent structure being detrimentally affected by adsorbed water. This applies particularly to MOF structures, where the metallic / organic constituents are in coordination with one another. In contrast, only carbon bonds are involved in the case of NPS, and of porous carbon cuboids (PCC-1).[18] Therefore, inspecting the list, only MOF-801, A520, $AlPO_4$, CAU-10, PCC-1 and NPS appear to satisfy the required criteria of low desorption temperature and high stability over multiple regeneration cycles. An important advantage of the MOFs is the ability to tightly control their pore size facilitated by a wide selection of molecular components of various types and sizes. In contrast, porosity of NPS is fixed and inherent to the material and process, offering only little control, at least at this point of their development.

It should be noted that adsorption kinetics have not been included in Table 6, the reason being the challenging task of comparing such data among published literature studies. Rigorously identical experimental conditions are in principle required to allow valid comparison, but kinetics are highly dependent on relative pressure and temperature, humid air flow rate, sorbent particle size, packing porosity and how the adsorbent contacts the humid air (via diffusion or through a powder bed) .[53,54]

A clearly vital aspect of water adsorption on a truly industrial scale is the ability to cost-effectively synthesize large quantities of the sorbent material. The NPS synthesis process being relatively simple, it has been scaled-up to tens of grams in the laboratory. A full-scale installation could deliver kilograms, potentially up to several metric tons of NPS adsorbent at reasonable cost: Its primary constituents, resorcinol (R) and formaldehyde (F), are abundant industrial chemicals, with respective costs per ton of US$ 1,700 and US$ 500.[55,56] Based on these, on solvent, and energy requirements, it is estimated that NPS material production would cost between US$ 15 and 40 per kg (see Table S2). In comparison, silica gel, a well-established and widely available sorbent, can be purchased for less than US$ 10 per kg. However, silica gel requires higher desorption temperature (>200 °C) and exhibits lower stability over adsorption/desorption cycles.[57] On the other hand, MOFs currently face scalability challenges, because their crystallization is a slow batch process that calls for highly controlled temperature and pressure conditions. For example, Furukawa et al. described a 6-hour long synthesis to produce 10 g of MOF-801, followed by a 7-day period of rinsing and drying.[16] In addition to slow synthesis, MOF precursors can be expensive, especially their metallic constituent. Solely basing the estimation from the required precursors, MOF-801 could cost nearly US$ 100 per kg, while being commercially available at small scale for US$ 100 per gram.[58] One can note, however, that new synthesis processes are being

developed to help improve the scalability and costs of MOF production, such as earlier-mentioned electrochemistry or assistance by microwave power.[15]

4. Conclusion

Nanoporous sponges (NPS) have been prepared based on resorcinol-formaldehyde (R-F) resins; after undergoing heat treatments and functionalization steps, they are here referred to as NPS, N-NPS, O-NPS and NO-NPS. These sorbents have been shown to possess a fine, narrow pore size distribution centered near 1.5 nm. They exhibit good water adsorption performance, especially O-NPS, namely 0.28 $g \cdot g^{-1}$ of adsorbent at P/Psat = 0.90 and 0.14 $g \cdot g^{-1}$ at P/Psat = 0.40, values that were found to be stable over at least five regeneration cycles, many more in some cases. The scalability of material production has been demonstrated with non-functionalized NPS, whereby samples maintained their performance among quantities ranging from tens of milligrams to tens of grams. Fitting measured adsorption isotherms with the theoretical model of Do and Do has allowed us to convincingly establish surface-bonded hydroxyl groups as the primary adsorption sites. Additional surface oxidation led to still higher OH concentrations and to further improved water adsorption performance. Conversely, nitrogen addition reduced the concentration of OH groups and modified the material's porosity, hence resulting in undesirable H3 hysteresis in the corresponding isotherms. Perspectives for further improving NPS sorbents include means to better control OH group concentrations during synthesis. Controlling heat- and mass transfer of water vapor through NPS micro particles, and inside their pores, will lead to better account for promoting large-scale practical application. Further work is required to assess the thermodynamic behavior and kinetics data of our NPS samples to reinforce our comparisons to other available sorbents.

5. Acknowledgements

The authors acknowledge financial support from the Natural Sciences and Engineering Research Council of Canada (NSERC grant CRD-522391), Prima (grant R16-46-003) and Awn Nanotech Inc. We would like to thank Adrien D'Oliveira from Polytechnique Montreal for performing BET measurements on our samples, Sonia Blais from Université de Sherbrooke for CHN analyses, and the Centre for Characterization and Microscopy of Materials $(CM)^2$ at Polytechnique Montreal for SEM analysis.

6. Conflict of interest

The authors U. Legrand, R. Boudreault and J. R. Tavares have filed a patent based on the findings described in the present article, and thus acknowledge their personal financial interest in this research. R. Boudreault is the CEO of Awn Nanotech Inc. the industrial partner supporting this research. This potential conflict of interest has not led any of the co-authors to bias or otherwise modify any of the methods and/or results reported here.

7. References

1. FAO. *Highlands and Drylands*. *Fao* (2011).
2. Gabbatiss, J. Cape Town is approaching drought 'Day Zero' and climate change could be to blame. *2018* https://www.independent.co.uk/environment/cape-town-drought-day-zero-climate-change-global-warming-south-africa-a8236511.html.
3. Wada, Y. *et al.* Global depletion of groundwater resources. *Geophys. Res. Lett.* **37**, 1–5 (2010).
4. Zotalis, K., Dialynas, E. G., Mamassis, N. & Angelakis, A. N. Desalination technologies: Hellenic experience. *Water (Switzerland)* **6**, 1134–1150 (2014).
5. Thiel, G. P. Salty solutions. *Phys. Today* **68**, 66–67 (2015).
6. Wahlgren, R. V. Atmospheric water vapour processor designs for potable water production: A review. *Water Res.* **35**, 1–22 (2001).
7. Horikawa, T., Do, D. D. & Nicholson, D. Capillary condensation of adsorbates in porous materials. *Adv. Colloid Interface Sci.* **169**, 40–58 (2011).

8. Sundararajan, M. & Chen, G. X-ray Scattering Study of Capillary Condensation in Mesoporous Silica. https://www.slideshare.net/MayurSundararajan/apspresentationmayur.

9. Szoszkiewicz, R. & Riedo, E. Nucleation time of nanoscale water bridges. *Phys. Rev. Lett.* **95**, 1–4 (2005).

10. Grosman, A. & Ortega, C. Capillary condensation in porous materials. Hysteresis and interaction mechanism without pore blocking/percolation process. *Langmuir* **24**, 3977–3986 (2008).

11. Rieth, A. J., Yang, S., Wang, E. N. & Dincă, M. Record Atmospheric Fresh Water Capture and Heat Transfer with a Material Operating at the Water Uptake Reversibility Limit. *ACS Cent. Sci.* **3**, 668–672 (2017).

12. Kalmutzki, M. J., Diercks, C. S. & Yaghi, O. M. Metal–Organic Frameworks for Water Harvesting from Air. *Adv. Mater.* **30**, 1–26 (2018).

13. Canivet, J., Fateeva, A., Guo, Y., Coasne, B. & Farrusseng, D. Water adsorption in MOFs: Fundamentals and applications. *Chem. Soc. Rev.* **43**, 5594–5617 (2014).

14. Babu, R., Roshan, R., Kathalikkattil, A. C., Kim, D. W. & Park, D. W. Rapid, Microwave-Assisted Synthesis of Cubic, Three-Dimensional, Highly Porous MOF-205 for Room Temperature CO2 Fixation via Cyclic Carbonate Synthesis. *ACS Appl. Mater. Interfaces* **8**, 33723–33731 (2016).

15. Rubio-Martinez, M. *et al.* New synthetic routes towards MOF production at scale. *Chem. Soc. Rev.* **46**, 3453–3480 (2017).

16. Furukawa, H. *et al.* Water adsorption in porous metal-organic frameworks and related materials. *J. Am. Chem. Soc.* **136**, 4369–4381 (2014).

17. Biswal, B. P. *et al.* Pore surface engineering in porous, chemically stable covalent organic frameworks for water adsorption. *J. Mater. Chem. A* **3**, 23664–23669 (2015).

18. Hao, G. P. *et al.* Unusual ultra-hydrophilic, porous carbon cuboids for atmospheric-water capture. *Angew. Chemie - Int. Ed.* **54**, 1941–1945 (2015).

19. Zhou, X., Lu, H., Zhao, F. & Yu, G. Atmospheric Water Harvesting : A Review of Material and Structural Designs. *ACS Mater. Lett.* **2**, 671–684 (2020).

20. Yu, J. *et al.* Simple fabrication of an ordered nitrogen-doped mesoporous carbon with resorcinol-melamine-formaldehyde resin. *Microporous Mesoporous Mater.* **190**, 117–127 (2014).

21. Wen, Z. B. *et al.* An activated carbon with high capacitance from carbonization of a resorcinol-formaldehyde resin. *Electrochem. commun.* **11**, 715–718 (2009).

22. Wang, Y., Chang, B., Guan, D. & Dong, X. Mesoporous activated carbon spheres derived from resorcinol-formaldehyde resin with high performance for supercapacitors. *J. Solid State Electrochem.* **19**, 1783–1791 (2015).

23. Civioc, R., Lattuada, M., Koebel, M., Galmarini, S. Monolithic resorcinol-formaldehyde alcogels and their corresponding nitrogen-doped activated carbons. *Journal of Sol-Gel*

Science and Technology. **95** (2020).

24. Velasco, L. F., Snoeck, D., Mignon, A. *et al.* Role of the surface chemistry of the adsorbent on the initialization step of the water sorption process. *Carbon*, **106**, 284-288 (2016).

25. Huber, L., Ruch, P., Hauert, R., *et al.* Monolithic nitrogen-doped carbon as a water sorbent for high-performance adsorption cooling. *RCS Adv.* **6**, 25267-25278 (2016).

26. Huber, L., Ruch, P., Hauert, R., *et al.* Water sorption behavior of physically and chemically activated monolithic nitrogen doped carbon for adsorption cooling. *RCS Adv.* **6**, 80729-80738 (2016).

27. Huber, L., Hauser, S. B., Brendlé, E., *et al.* The effect of activation time on water sorption behavior of nitrogen-doped, physically activated, monolithic carbon for adsorption cooling. *Microporous and Mesoporous Materials,* **276**, 239-250 (2019).

28. Horikawa, T., Hayashi, J. & Muroyama, K. Controllability of pore characteristics of resorcinol-formaldehyde carbon aerogel. *Carbon N. Y.* **42**, 1625–1633 (2004).

29. Pascone, P.-A., Campos, J. de, Meunier, J.-L. & Berk, D. Iron Incorporation on Graphene Nanoflakes for the Synthesis of a Non-noble Metal Fuel Cell Catalyst. *Appl. Catal. B Environ.* **193**, 9–15 (2016).

30. Do, D. D. & Do, H. D. A model for water adsorption in activated carbon. *Carbon N. Y.* **38**, 767–773 (2000).

31. Neitsch, M., Heschel, W. & Suckow, M. Water vapor adsorption by activated carbon: A modification to the isotherm model of Do and Do [6]. *Carbon N. Y.* **39**, 1437–1438 (2001).

32. Furmaniak, S., Gauden, P. A., Terzyk, A. P. & Rychlicki, G. Water adsorption on carbons - Critical review of the most popular analytical approaches. *Adv. Colloid Interface Sci.* **137**, 82–143 (2008).

33. Do, D. D., Junpirom, S. & Do, H. D. A new adsorption-desorption model for water adsorption in activated carbon. *Carbon N. Y.* **47**, 1466–1473 (2009).

34. Shiraishi, Y. *et al.* Resorcinol–formaldehyde resins as metal-free semiconductor photocatalysts for solar-to-hydrogen peroxide energy conversion. *Nat. Mater.* **18**, 985–993 (2019).

35. Onodera, T. *et al.* Analysis of forming process of nitrogen-doped carbon catalyst derived from Fe 1,10-phenanthroline compound and its oxygen reduction reaction activity. *Catal. Commun.* **43**, 66–71 (2014).

36. Alothman, Z. A. A review: Fundamental aspects of silicate mesoporous materials. *Materials (Basel).* **5**, 2874–2902 (2012).

37. Kutarov, V. V., Tarasevich, Y. I., Aksenenko, E. V. & Ivanova, Z. G. Adsorption hysteresis for a slit-like pore model. *Russ. J. Phys. Chem. A* **85**, 1222–1227 (2011).

38. Furmaniak, S. *et al.* Water at curved carbon surface: Mechanisms of adsorption revealed

by first calorimetric study. *J. Phys. Chem. C* **119**, 2703–2715 (2015).

39. Ludwig, R. Water: From Clusters to the Bulk. *Angew. Chemie Int. Ed.* **40**, 1808–1827 (2001).

40. Kim, H. *et al.*, Characterization of Adsorption Enthalpy of Novel Water-Stable Zeolites and Metal-Organic Frameworks. Sci Rep **6**, 10097 (2016).

41. Yang, SuKim, H. *et al.* Water harvesting from air with metal-organic framework powered by natural sunlight. *Science (80-.).* **434**, 430–434 (2017).

42. Thommes. M. *et al.*, Combining Nitrogen, Argon, and Water Adsorption for Advanced Characterization of Ordered Mesoporous Carbons (CMKs) and Periodic Mesoporous Organosilicas (PMOs). *Langmuir* **29**, 48, 14983-14902 (2013).

43. Majchrzak-Kucęba, I. & Bukalak-Gaik, D. Regeneration performance of metal–organic frameworks: TG-Vacuum tests. *Journal of Thermal Analysis and Calorimetry* vol. 125 1461–1466 (2016).

44. Llewellyn, P. L. *et al.* Water Sorption on Mesoporous Aluminosilicate MCM-41. *Langmuir* **11**, 574–577 (1995).

45. Cui, S. *et al.*, Metal-Organic Frameworks as advanced moisture sorbents for energy-efficient high temperature cooling. *Sci Rep* **8**, 15284 (2018).

46. Henninger, S. K. *et al.*, Water adsorption characteristics of novel materials for heat transformation applications. *Appplied Thermal Engineering* **30**, 13, 1692-1702 (2010).

47. Solovyeva, M. V., Gordeeva, L. G., Krieger, T. A. & Aristov, Y. I. MOF-801 as a promising material for adsorption cooling: Equilibrium and dynamics of water adsorption. *Energy Convers. Manag.* **174**, 356–363 (2018).

48. Fröhlich, D. *et al.* Water adsorption behaviour of CAU-10-H: A thorough investigation of its structure-property relationships. *J. Mater. Chem. A* **4**, 11859–11869 (2016).

49. Cho, K. *et al.* Development of highly performing water-adsorption chiller using new aluminophosphate as water adsorbent. *12th IEA Heat Pump Conference* O.4.5.3 (2017).

50. Reinsch, H. *et al.* A new Al-MOF based on a unique column-shaped inorganic building unit exhibiting strongly hydrophilic sorption behaviour. *Chem. Commun.* **48**, 9486–9488 (2012).

51. Sayilgan, Ş. Ç., Mobedi, M. & Ülkü, S. Effect of regeneration temperature on adsorption equilibria and mass diffusivity of zeolite 13x-water pair. *Microporous Mesoporous Mater.* **224**, 9–16 (2016).

52. Decoste, J. B. *et al.* The effect of water adsorption on the structure of the carboxylate containing metal-organic frameworks Cu-BTC, Mg-MOF-74, and UiO-66. *J. Mater. Chem. A* **1**, 11922–11932 (2013).

53. Hanikel, N. *et al.* Rapid Cycling and Exceptional Yield in a Metal-Organic Framework Water Harvester. *ACS Cent. Sci.* **5**, 1699–1706 (2019).

54. LaPotin, A., Kim, H., Rao, S. R. & Wang, E. N. Adsorption-Based Atmospheric Water Harvesting: Impact of Material and Component Properties on System-Level Performance. *Acc. Chem. Res.* **52**, 1588–1597 (2019).

55. Resorcinol Market. https://www.grandviewresearch.com/industry-analysis/resorcinol-market.

56. Formaldehyde Market. https://www.pharmacompass.com/price/formaldehyde.

57. Wang, D. *et al.* Investigation of adsorption performance deterioration in silica gel–water adsorption refrigeration. *Energy Conversion and Management* **58**, 157-162 (2012).

58. Nanoshel LLC. https://www.nanoshel.com/.